SPE-205884-MS

# Numerical RTA in Tight Unconventionals

Mathias Lia Carlsen, Whitson AS; Braden Bowie, Apache Corporation; Mohamad Majzoub Dahouk, Stian Mydland, Curtis Hays Whitson, and Ilina Yusra, Whitson AS



This paper was prepared for presentation at the 2021 SPE Annual Technical Conference and Exhibition held in Dubai, UAE, 21 - 23 September 2021.



## Abstract

We extend the numerically-assisted RTA workflow proposed by Bowie and Ewert (2020) to (a) *all* fluid systems and (b) finite conductivity fractures. The simple, fully-penetrating planar fracture model proposed is a useful numerical symmetry element model that provides the basis for the work presented in this paper. Results are given for simulated and field data.

The linear flow parameter (LFP) is modified to include porosity (LFP'=LFP$\sqrt{\varphi}$). The original (surface) oil in place (OOIP) is generalized to represent both reservoir oil and reservoir gas condensate systems, using a consistent initial total formation volume factor definition ($B_{ti}$) representing the ratio of a reservoir HCPV containing surface oil in a reservoir oil phase, a reservoir gas phase, or both phases.

With known (a) well geometry, (b) fluid initialization (PVT and water saturation), (c) relative permeability relations, and (d) bottomhole pressure (BHP) time variation (above and below saturation pressure), three fundamental relationships exist in terms of LFP' and OOIP. Numerical reservoir simulation is used to define these relationships, providing the foundation for numerical RTA, namely that wells: (1) with the same value of LFP', the gas, oil and water surface rates will be identical during infinite-acting (IA) behavior; (2) with the same ratio LFP'/OOIP, producing GOR and water cut behavior will be identical for all times, IA and boundary dominated (BD); and (3) with the same values of LFP' and OOIP, rate performance of gas, oil, and water be identical for all times, IA and BD. These observations lead to an efficient, semi-automated process to perform rigorous RTA, assisted by a symmetry element numerical model.

The numerical RTA workflow proposed by Bowie and Ewert solves the inherent problems associated with complex superposition and multiphase flow effects involving time and spatial changes in pressure, compositions and PVT properties, saturations, and complex phase mobilities.

The numerical RTA workflow decouples multiphase flow data (PVT, initial saturations and relative permeabilities) from well geometry and petrophysical properties ($L$, $x_f$, $h$, $n_f$, $\varphi$, $k$), providing a rigorous yet efficient and semi-automated approach to define production performance for many wells.

Contributions include a technical framework to perform numerical RTA for unconventional wells, irrespective of fluid type. A suite of key diagnostic plots associated with the workflow is provided, with synthetic and field examples used to illustrate the application of numerical simulation to perform rigorous RTA. Semi-analytical models, time, and spatial superposition (convolution), pseudopressure and pseudotime transforms are not required.

## Introduction

RTA methods to correct for superposition and multiphase flow effects have been studied extensively in the past. *Analytically*[1] correcting for the *combined* effect of both superposition and multiphase flow at the same time ("multiphase superposition") is not possible, as one needs to know saturations and PVT properties as a function of space for all times. Multiple cycles of hysteresis in a multiphase, complex PVT and relative permeability system, are *impossible* to handle analytically[2] (Jones 1985). The only way to get that information is a complete numerical solution with the actual bottomhole pressure history.

Bowie and Ewert (2020) introduced the concept of numerically assisted RTA for oil reservoirs to handle the inherent problems associated with classical industry-standard RTA, namely the proper, *combined* handling of:

- Rigorous superposition, describing hysteresis effects caused by widely changing pressures and rates, especially important during the early, infinite acting period.
- Multiphase flow effects, exhibiting large and discountinous changes in compressibility, viscosity, formation volume factors and relative saturations with pressure.

In this paper, we will look closer at the workflow proposed by Bowie and Ewert (2020), and

- generalize the workflow for *all* fluid systems[3], not only oil reservoirs.
- incorporate the use of finite conductivity fractures (low $F_{cd}$) consistently into the workflow.
- include porosity in the definition of a modified linear flow parameter, LFP', to allow for changes in porosity in the workflow.
- introduce the concept of "cumulative LFP's" to reduce noise.
- validate the workflow with both simulated data and real field data.

## Underlying assumptions – 1D Reservoir Model

The theory presented in this paper assumes a so-called "symmetry element" model, in which the underlying numerical model is representing one-quarter of a fracture. This is highlighted by the red-lined box in **Fig. 1**. The model is "1 dimensional", as there are no flow contributions beyond the fractips ($x_f = x_e$) or beyond the frac height ($h_f = h$). Hence, there is only one no-flow boundary, resulting in two dominant flow regimes over time; (1) infinite acting (IA) linear flow, followed by (2) boundary dominated (BD) flow. In this study, only one permeability zone assumed is assumed, i.e., no enhanced-permeability fracture region near the wellbore and hydraulic fracture. Still, most of the underlying concepts presented in this paper are also relevant for more complex reservoir geometries (layered systems, dual permeability regions, inclusion of non-stimulated matrix).

[1] In this context, "analytical" is referring to linearization of partial differential equations.

[2] To do that, one would need to know the "reservoir integral pseudopressure", which means knowing the entire numerical solution everywhere. This is the reason, for instance, that Clarkson et al (2019) leverages a calibrated simulation model as an input to a proposed multiphase correction methodology, as it is required to accurately estimate average pressures and saturations in the three flow regions they are integrating over.

[3] Except for dry gas reservoirs

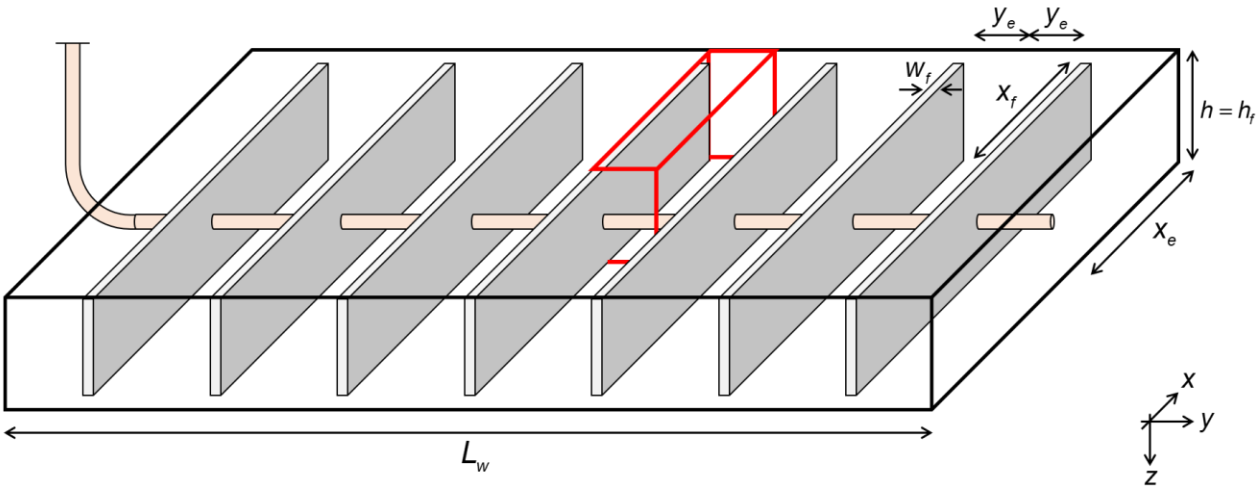


Fig. 1— Wellbox model assumed in this paper.

## RTA Fundamentals

Traditional RTA for tight unconventional resources involves plotting rate normalized pressure (RNP) versus square root of time, [$(p_i\text{-}p_{wf})/q_o$ *vs.* $\sqrt{t}$], commonly referred to as the "square-root-of-time plot". For single-phase oil flow at constant bottomhole pressure, the square-root-of-time plot exhibits a straight line with constant slope and zero intercept during IA, linear flow, as shown in **Fig. 2**. Deviation from the straight line indicates the end of infinite acting, linear flow. Obtaining the correct time to end of linear flow ($t_{elf}$) is key to solving for meaningful reservoir parameters such as permeability ($k$) and stimulated surface area ($A$).

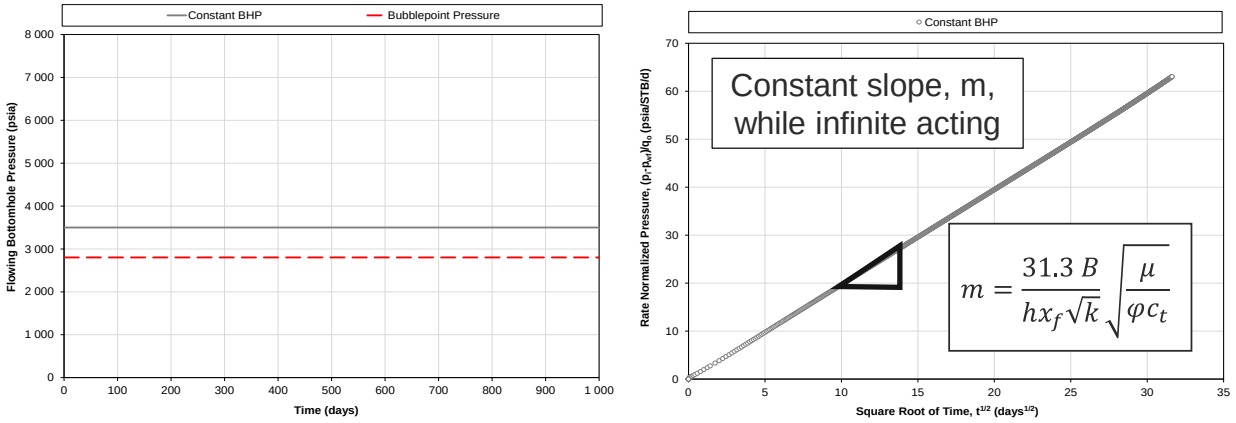


Fig. 2 — (a) Bottomhole pressure higher than the bubblepoint (ideal, single-phase oil flow).
(b) The "square root of time" plot exhibits a constant slope during infinite acting, linear flow.

As described by Bowie and Ewert (2020), deviations from the ideal, straight-line behavior during IA, linear flow are caused by superposition effects. This is even observed for flow under single-phase conditions, as shown in **Fig. 3**. Significantly changing BHPs, as exemplified here with step changes, introduce multiple straight lines on the square root of time plot. Such BHP variations often cause significant departure from the theoretical linear trend of the square-root-of-time plot, when working with real data.

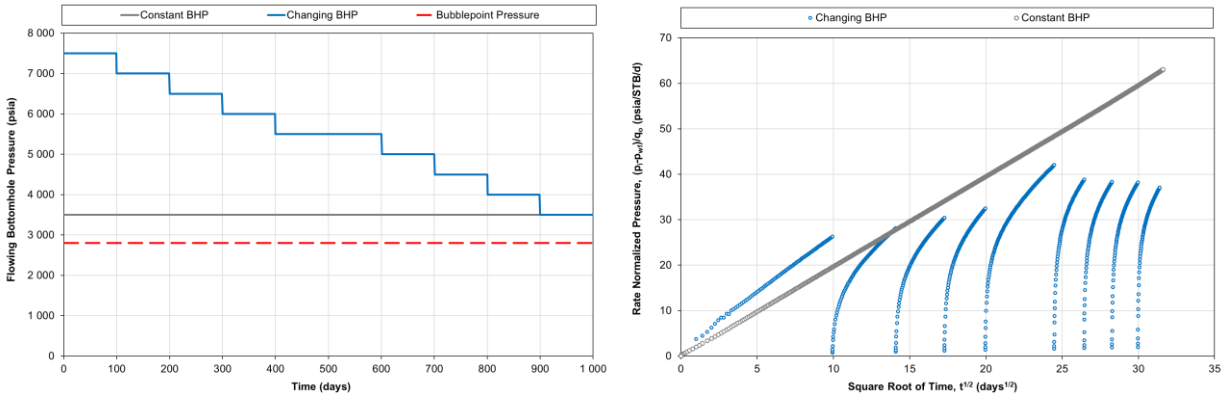


Fig. 3—(a) Superposition effects (i.e. changing rates and pressures) are introduced with a radically changing bottomhole pressure profile with time. (b) The "square root of time" plot exhibits several slopes when exposed to superposition effects, even when being in transient.

In addition to the superposition effects, multiphase flow effects are introduced as the bottomhole pressure drops below the saturation pressure. **Fig. 4** shows the square root of time plot for the same reservoir simulation model controlled on two different drawdown profiles, dropping below the bubblepoint at two different times. It is important to emphasize that the simulation model is in infinite acting, linear flow throughout the entire presented history. However, deviation from straight line behavior is observed as the bottomhole pressure drops below the bubblepoint pressure and multiphase flow effects become apparent. This combined effect of superposition and multiphase flow causes a deviation from straight line behavior that is not caused by boundary effects but could be misinterpreted as such. Incorrectly picking a too small time to end of linear flow would lead to a short frac half-length and high permeability, and the erroneous conclusion of proceeding with tight well spacing.

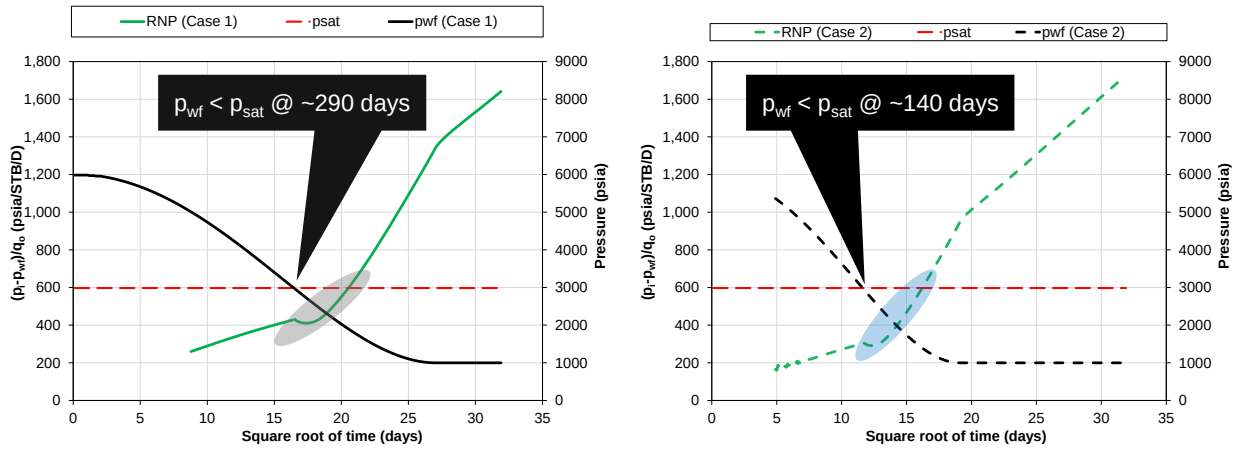


Fig. 4— (a) Bottomhole pressure drops below saturation pressure after about 290 days, causing a deviation from straight line behavior. (b) Bottomhole pressure drops below saturation pressure after about 140 days, causing a deviation from straight line behavior.

## Numerically Assisted RTA: Key Geometric Variables

To understand the numerically assisted RTA workflow outlined in this paper, the theoretical background must be presented and validated. To reduce the number of geometric variables, the *modified linear flow parameter* (LFP')[4] and *original oil in place* (OOIP) are defined as follows:

$$LFP' = LFP\sqrt{\varphi} = 4n_f x_f h\sqrt{k}\sqrt{\varphi} \tag{1}$$

$$OOIP = \frac{2x_f Lh\varphi(1 - S_{wi})}{B_{ti}} \tag{2}$$

The introduction of *initial total formation volume factor* ($B_{ti}$) generalizes the workflow proposed by Bowie & Ewert (2020) to all fluid types, for both initially undersaturated and (two-phase) saturated conditions[5]. $B_{ti}$ is defined as

$$B_{ti} = \frac{S_{oi} + S_{gi}}{\frac{S_{oi}}{B_{oi}} + \frac{S_{gi}}{B_{gdi}/r_{si}}} \tag{3}$$

which for an undersaturated oil reservoir ($S_{gi}$= 0) will simplify to $B_o$ and for an undersaturated gas reservoir ($S_{oi}$= 0) will simplify to $B_{gd}/r_s$. For a two-phase saturated case, the $B_{ti}$ will represent a saturation weighted oil FVF[6]. As mentioned earlier, $B_{ti}$ represents the ratio of a reservoir HCPV containing surface oil in a reservoir oil phase, a reservoir gas phase, or both phases.

## Numerically Assisted RTA: Relationships between LFP', OOIP and Well Performance

For a given fluid initialization (PVT and $S_{wi}$), relative permeability curves, and bottomhole-pressure profile versus time, three fundamental relationships exist between LFP', OOIP, and well performance[7].

1. Wells with the *same LFP' yield the same well performance* during infinite acting, linear flow. If the OOIP is different, time to end of linear flow is different, and the well performance diverges as the well enters transitional (to-BD) flow. This relationship is exemplified in **Fig. 5.**
2. Wells with the same *LFP'*/OOIP ratio yield the same producing GOR and water cuts for all times (relative rates), regardless of the actual value of LFP and OOIP. This fundamental relationship is exemplified in **Fig. 6**.
3. Wells with the *same LFP' and OOIP yield the same well performance for all times and all flow regimes*. In other words, if LFP' and OOIP are the same for two wells, the well performance is identical (rates, cumulatives, GOR, water cuts), independent of time and flow regime (IA or BD). This fundamental relationship is exemplified in **Fig. 7**.

These relationships provide the foundation for numerical RTA, and lead to an efficient, semi-automated process to perform rigorous RTA, assisted by a symmetry element numerical model.

[4] Note that we are strictly differentiating between LFP' and LFP in this paper.
[5] Except for dry gases. There is a special section on dry gases later in this paper.
[6] A "cheat sheet" with all the relevant equations are provided in **Appendix A**.
[7] Remember that the well geometry assumed here is the same as outlined in Fig. 1.

## Same LFP', same Infinite Acting (IA) Performance

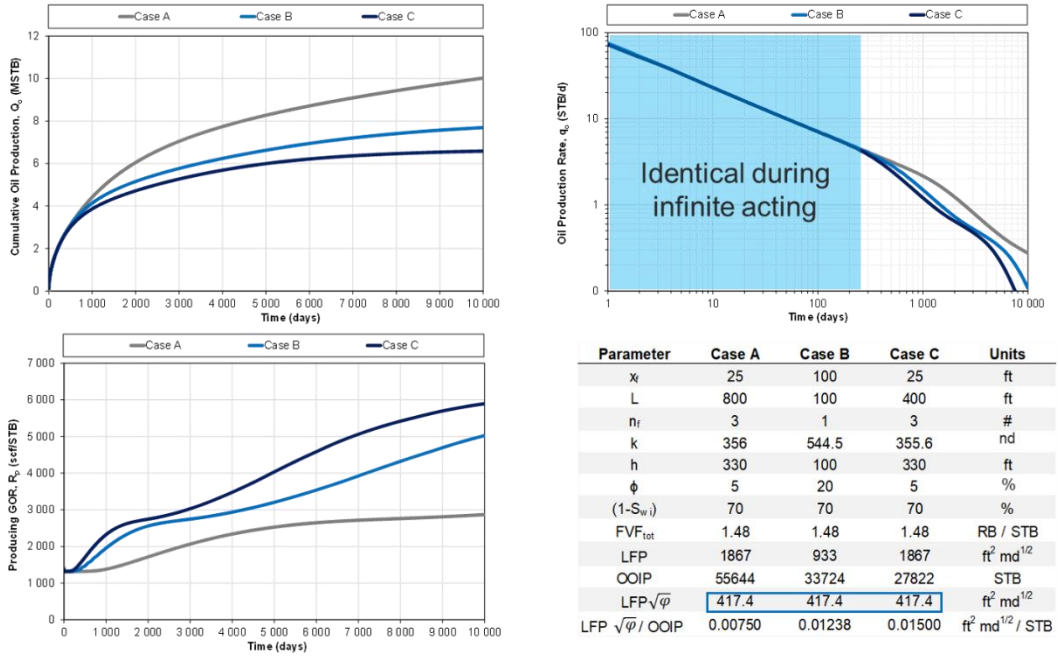


| Parameter | Case A | Case B | Case C | Units |
|---|---|---|---|---|
| $x_f$ | 25 | 100 | 25 | ft |
| L | 800 | 100 | 400 | ft |
| $n_f$ | 3 | 1 | 3 | # |
| k | 356 | 544.5 | 355.6 | nd |
| h | 330 | 100 | 330 | ft |
| $\phi$ | 5 | 20 | 5 | % |
| $(1-S_{wi})$ | 70 | 70 | 70 | % |
| $FVF_{tot}$ | 1.48 | 1.48 | 1.48 | RB / STB |
| LFP | 1867 | 933 | 1867 | $ft^2\ md^{1/2}$ |
| OOIP | 55644 | 33724 | 27822 | STB |
| $LFP\sqrt{\varphi}$ | 417.4 | 417.4 | 417.4 | $ft^2\ md^{1/2}$ |
| $LFP\ \sqrt{\varphi}$ / OOIP | 0.00750 | 0.01238 | 0.01500 | $ft^2\ md^{1/2}$ / STB |

Fig. 5— Example of three different cases with the same LFP' = LFP$\sqrt{\varphi}$, but different OOIP. Note how the performance is identical during the infinite, acting linear flow period and diverges when entering boundary dominated flow.

## Same LFP' and different OOIP, same relative rates (GOR and water cut)

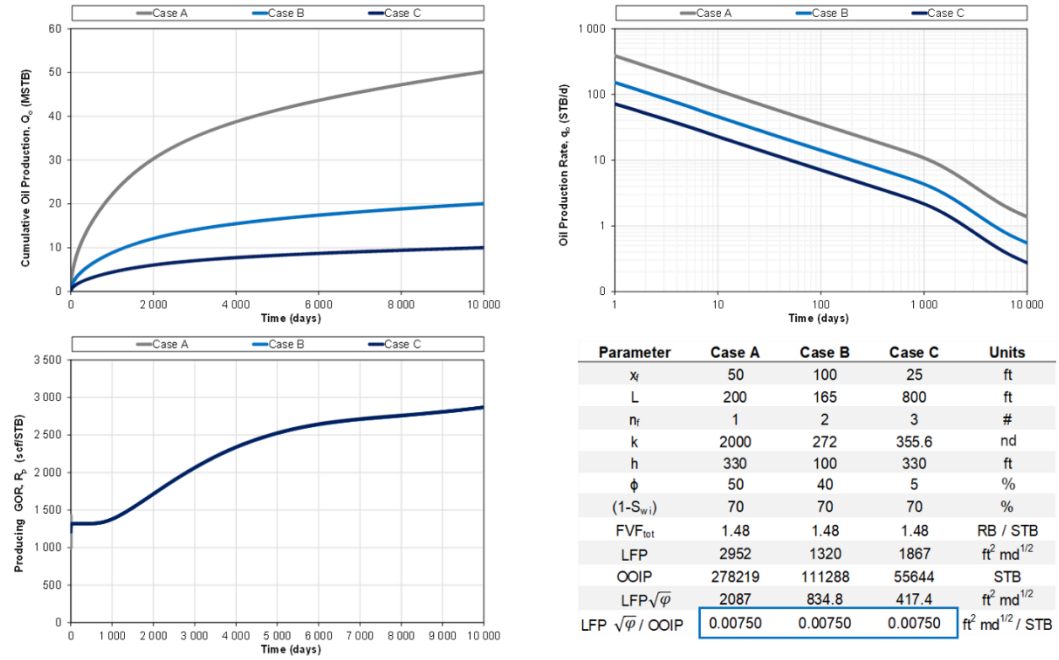


| Parameter | Case A | Case B | Case C | Units |
|---|---|---|---|---|
| $x_f$ | 50 | 100 | 25 | ft |
| L | 200 | 165 | 800 | ft |
| $n_f$ | 1 | 2 | 3 | # |
| k | 2000 | 272 | 355.6 | nd |
| h | 330 | 100 | 330 | ft |
| $\phi$ | 50 | 40 | 5 | % |
| $(1-S_{wi})$ | 70 | 70 | 70 | % |
| $FVF_{tot}$ | 1.48 | 1.48 | 1.48 | RB / STB |
| LFP | 2952 | 1320 | 1867 | $ft^2\ md^{1/2}$ |
| OOIP | 278219 | 111288 | 55644 | STB |
| $LFP\sqrt{\varphi}$ | 2087 | 834.8 | 417.4 | $ft^2\ md^{1/2}$ |
| $LFP\ \sqrt{\varphi}$ / OOIP | 0.00750 | 0.00750 | 0.00750 | $ft^2\ md^{1/2}$ / STB |

Fig. 6—. Example of three different cases with the same LFP'/OOIP ratio. Note that the relative rates are identical (here exemplified by GOR) for both infinite acting and boundary dominated flow. Also note that the performance differs by a constant multiplier.

**Same LFP' and OOIP, same performance**

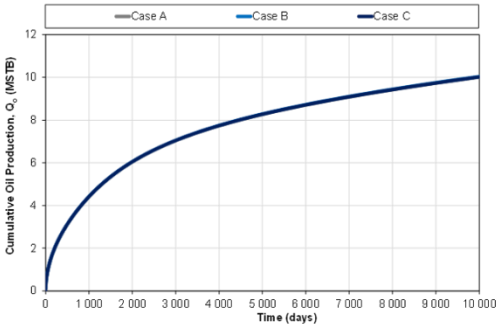


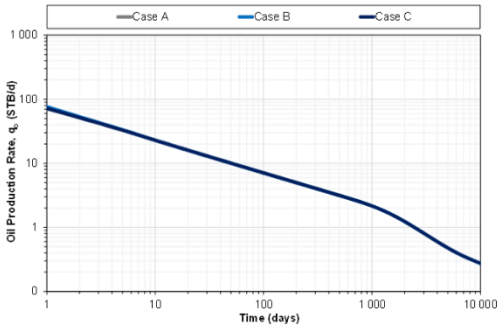


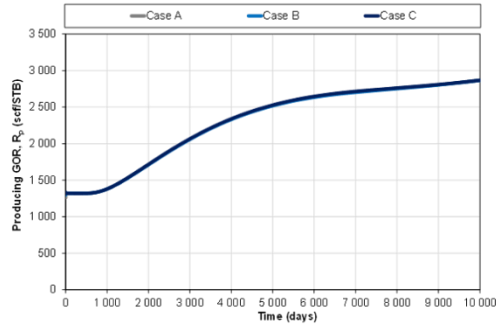


| Parameter | Case A | Case B | Case C | Units |
|---|---|---|---|---|
| $x_f$ | 330 | 100 | 25 | ft |
| L | 100 | 165 | 800 | ft |
| $n_f$ | 1 | 1 | 3 | # |
| k | 100 | 545 | 356 | nd |
| h | 100 | 100 | 330 | ft |
| $\phi$ | 10 | 20 | 5 | % |
| $(1-S_{wi})$ | 70 | 70 | 70 | % |
| $FVF_{tot}$ | 1.48 | 1.48 | 1.48 | RB / STB |
| LFP | 1320 | 933 | 1867 | $ft^2\ md^{1/2}$ |
| OOIP | 55644 | 55644 | 55644 | STB |
| $LFP\sqrt{\varphi}$ | 417.4 | 417.4 | 417.4 | $ft^2\ md^{1/2}$ |
| $LFP\ \sqrt{\varphi}$ / OOIP | 0.00750 | 0.00750 | 0.00750 | $ft^2\ md^{1/2}$ / STB |

Fig. 7— Example of three cases with the same LFP' and OOIP. Note thathe well performance is identical during both infinite acting and boundary dominated flow.

## Numerically Assisted RTA: Workflow

For completeness, the workflow proposed by Bowie and Ewert (2020) is restated, with a few minor modifications[8],

1. Create a numerical symmetry element model (the "template model") that is large enough to behave infinite acting (=large OOIP) for the entirety of the historical time of the well being analyzed. In practice, this means to create a single fracture, numerical model with a large ("infinite") distance to the closest boundary. Assign a relevant fluid initialization (PVT and $S_{wi}$) and relative permeability relations.
2. Run this "infinite acting model" controlled by (a) the well's actual measured bottomhole pressure [$p_{wf}$(t)], and (b) zero rate during shut-ins.
3. Calculate the ratio between the actual measured oil rates and infinite acting model oil rates: $r = q_{o,actual}/q_{o,IA}$. Alternatively, one can use the cumulative to reduce noise: $r = Q_{o,actual}/Q_{o,IA}$.
4. Calculate the daily LFP' by multiplying the daily ratio *r* (Step 3) with the known LFP' of the infinite acting, single fracture model (Step 1).
    a. a horizontal flat line indicates infinite acting, linear flow.
    b. deviation below this line represents transitional flow or boundary dominated flow.
    c. the magnitude of the horizontal trend indicates the LFP'.
5. Pick a "Representative LFP'" based on the early time "LFP'" plot. Remember that a flat, horizontal line is expected during infinite acting behavior.

[8] Main modifications are i) generalize LFP definition to include porosity, LFP' = LFP$\sqrt{\varphi}$, ii) emphasize that the workflow is valid for a given fluid initialization (PVT and $S_{wi}$) and relative permeability, iii) introduce the concept of "cumulative LFP", calculated by using the ratio of actual and model cumulatives and iv) specify well-control during shut-in periods.

6. Repeat steps 1-2 for multiple, smaller OOIP volumes (reduce distance to closest boundary in the "template model"). This results in several “type curves” with each its own LFP'/OOIP ratio.
7. Multiply each LFP'/OOIP ratio simulated in Step 6 by the “Representative LFP'” picked in Step 5.
8. Pick the OOIP stem that best matches the actual production data.

After picking an LFP’ and OOIP for a well, continue the exercise to resolve key reservoir parameters like permeability ($k$) and fracture half length ($x_f$). This is done by assuming a well lateral length ($L$), number of fractures ($n_f$), reservoir height ($h$) and porosity ($\varphi$). Reorder **Eqs. 1-2**, as follows:

$$k = \left[\frac{(LFP\sqrt{\varphi}/OOIP)(1-S_{wi})\sqrt{\varphi}L}{2B_t n_f}\right]^2 \tag{4}$$

$$x_f = \frac{LFP}{4n_f h\sqrt{k}} \tag{5}$$

These resolved parameters can be used directly into a numerical reservoir simulator, and as the workflow is already leveraging a numerical model, a full consistency between the RTA and numerical reservoir simulation model is guaranteed. In other words, if the numerical RTA provides good results, then the first run of the numerical reservoir simulator should yield a very history match. From a high-level perspective, the numerical RTA workflow is illustrated in **Fig. 8**.

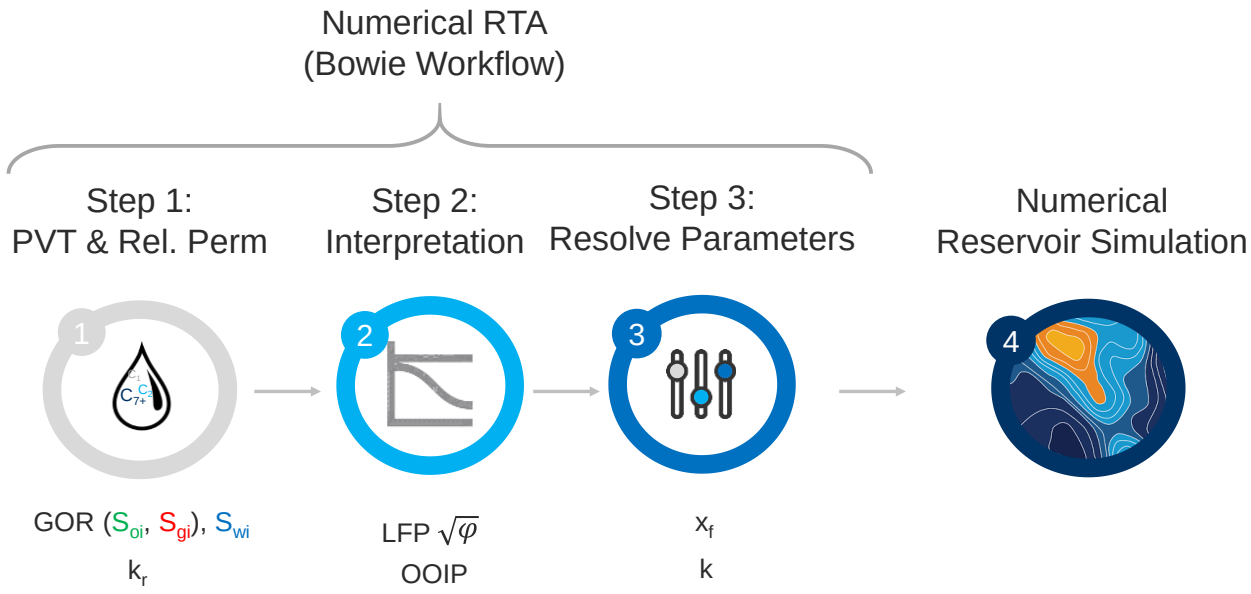


Fig. 8— The numerical RTA workflow.

One might argue that the uncertainty in some of the input parameters to this approach is too large, especially the number of fractures and fracture height. In this case, the LFP’ and OOIP parameters could still be used as is (“composite parameters”), which yet again can be tied to different completion practices, well spacing decisions and economics. In this sense, LFP’ and OOIP represent the parameters that can be uniquely derived from the production data, with the physical parameters in LFP’ and OOIP being non-unique.

## Numerically Assisted RTA: Synthetic Data

To verify the workflow, a synthetic oil well case is analyzed. The associated well and reservoir parameters are summarized in **Table 1**, resulting in an LFP' ~ 100,000 $ft^2md^{1/2}$ and OOIP ~ 3360 MSTB.

Table 1— Well and Reservoir Parameters.

| | | | | | | | | | | | |
|---|---|---|---|---|---|---|---|---|---|---|---|
| $p_{Ri}$ | 8000 | psia | $x_f$, $x_e$ | 400 | ft | $k_m$ | 200 | nd | $S_{org}$, $S_{wc}$, $S_{orw}$ | 20 | % |
| $T_R$ | 200 | F | $h_f$, h | 200 | ft | $\varphi_m$ | 5 | % | $S_{gc}$ | 5 | % |
| $R_{si}$ | 1000 | scf/STB | $L_w$ | 5000 | ft | $F_{CD}$ | 1000 | - | $k_{rocw}$, $k_{rwro}$, $k_{rgro}$ | 1 | - |
| $B_o$ | 1.472 | RB/STB | $N_f$ | 100 | # | $S_{wi}$ | 30 | % | $n_w$, $n_{ow}$, $n_{og}$, $n_g$ | 2 | - |

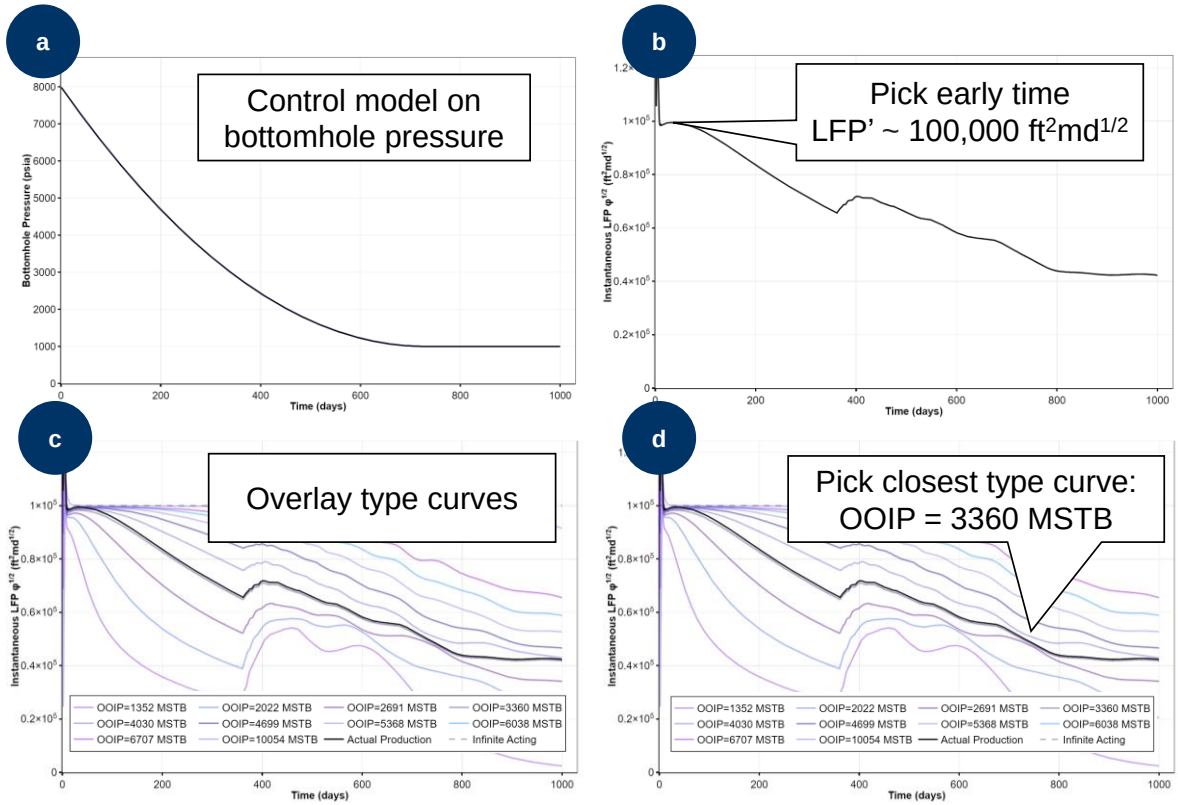


Fig. 9 — (a) control model on bottomhole pressure (b) calculate LFP' (c) overlay type curves (d) pick closest type curve.

**Numerical RTA workflow.** The well is controlled on a typical "shale" bottomhole pressure profile as illustrated in **Fig. 9a**, i.e., significantly declining bottomhole pressures until some constant value. First, the daily LFP' values are calculated as described in the previous section (step 1-4) and presented in **Fig. 9b**. This is the key diagnostic plot in the workflow. It is seen that the early LFP' values are flat around 100,000 $ft^2md^{1/2}$ (step 5). Secondly, the different OOIP type curves are overlaid onto the plot (step 6-7) as observed in **Fig. 9c**. Lastly, the OOIP stem that is closest to the observed data is picked (step 8), which is around 3360 days MSTB, as highlighted in **Fig. 9d**. With the LFP' and OOIP values selected, the values for $L$, $h$, $n_f$ and $\varphi$ provided in Table 1, Eqs. 4-5 can be used to back-calculate $k$ ~ 200 nd and $x_f$ ~ 400 ft.

**Cumulative LFP'.** Bowie and Ewert (2020) originally proposed to calculate the daily LFP' (step 3) by using the ratio of daily rates ($q_{actual}$ / $q_{model}$), resulting in the *instantaneous LFP'*. Alternatively, one can use the ratio of cumulatives produced until a given day ($Q_{actual}$ / $Q_{model}$) to reduce noisy data, resulting in the *cumulative LFP'*. For the abovementioned example, the cumulative LFP' is plotted over time in **Fig. 10**, and as observed the best-fit LFP' and OOIP are the same as the ones indicated from the instantaneous LFP'. The usefulness of this plot will be further emphasized when working with real data.

An alternative to reduce noise when working with real field data is to plot a *moving average* instantaneous LFP.

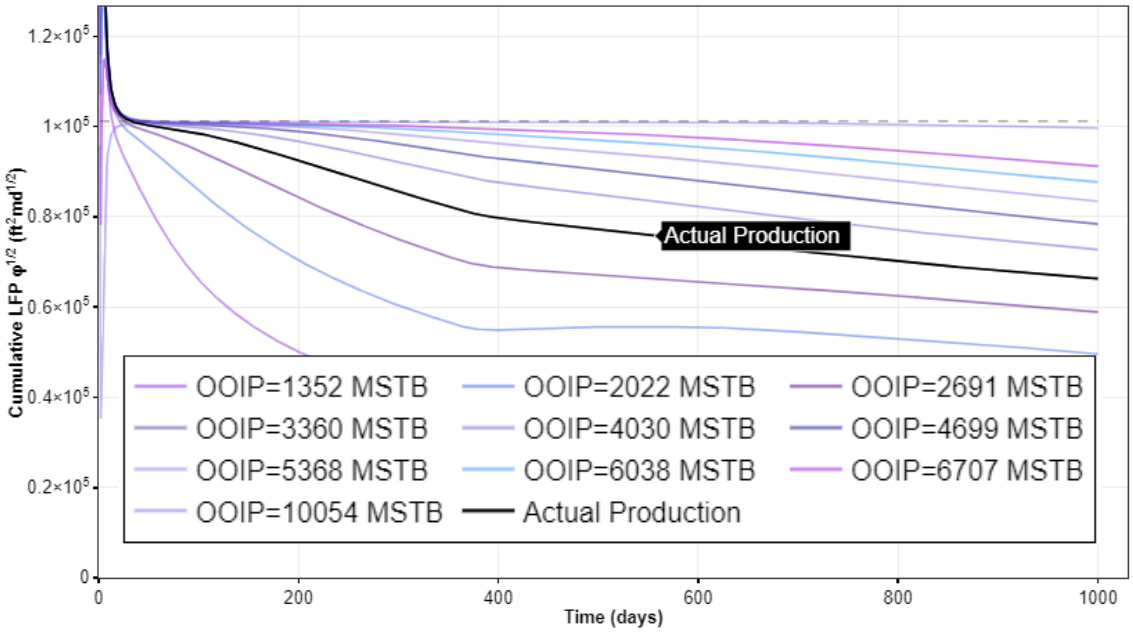


Fig. 10—Cumulative LFP' versus time for different OOIP numbers.

**Different Diagnostic Plots.** Once an LFP' is selected, the confidence in the corresponding OOIP value can be increased by analyzing several diagnostic plots at the same time, in addition to the LFP' plot itself. All the diagnostic plots should line up and indicate the same LFP' and OOIP. Some of the most useful plots are provided in **Fig. 11**.

For instance, if a certain LFP' and OOIP set provide a good match on the cumulative oil and gas diagnostic plots (Fig. 11a-b), it will guarantee a good history match, as long as the numerical RTA output is used consistently[9] in the following reservoir simulation exercise.

In addition, as outlined in detail by Jones (2016), different flow regimes can significantly impact GOR performance. For tight unconventional wells, exhibiting infinite acting flow, the producing GOR is a strong function of $p_{wf}$, while for wells exhibiting boundary dominated flow, the producing GOR is a strong function of *both* $p_{wf}$ and $p_{avg}$. Hence, it can be useful to look at the actual GOR and compare it to the predicted GOR exhibited by the different OOIP type curves (Fig. 11c). Similar analysis can be performed on the water cut performance (Fig. 11d). This is somewhat more challenging to use in practice with real data, as water cuts tend to be less impacted by flow regimes compared to for example GOR. That said, both the GOR and water cut examples provided in Fig. 11c-d further emphasize the fundamental, and important relationship between LFP' and OOIP, i.e. *two wells with the same ratio LFP'/OOIP, GOR and water cut behavior will be identical for all times, irrespective of flow regime (IA or BD).*

[9] LFP' and OOIP used as a basis for resolving parameters such as $x_f$ and $k$.

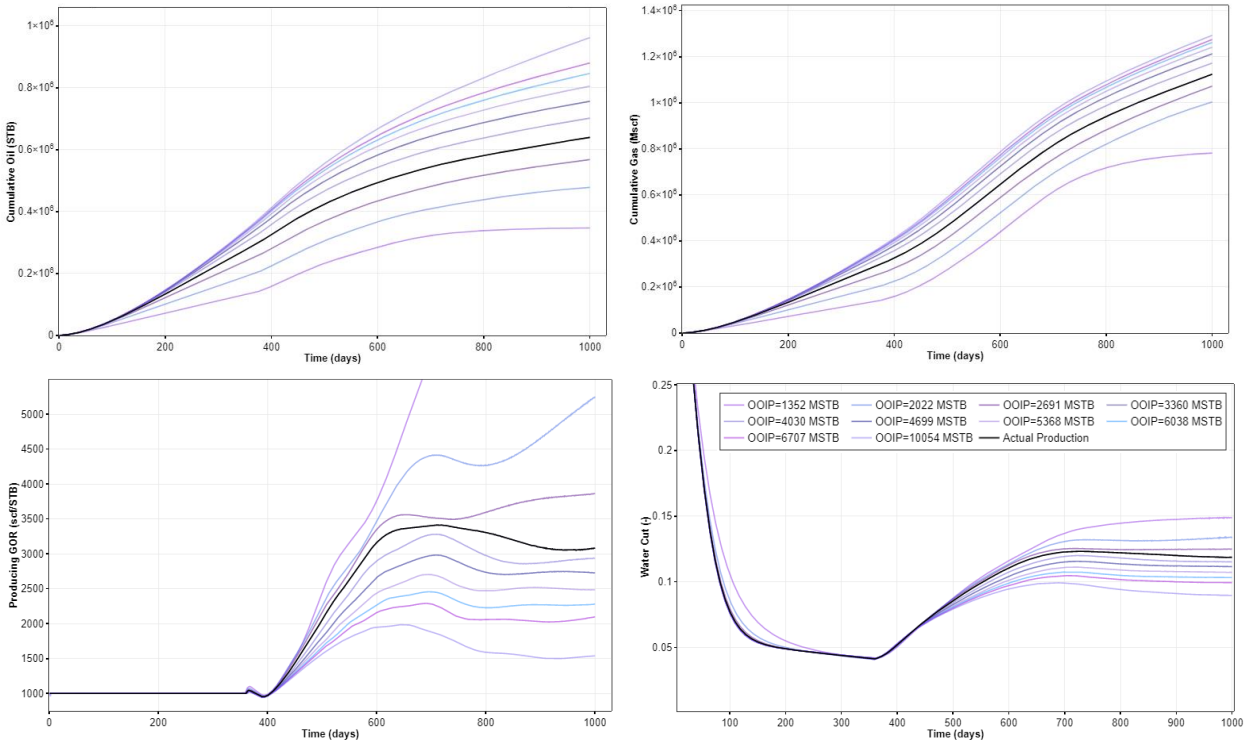


Fig. 11— (a) cumulative oil, (b) cumulative gas, (c) producing instantaneous GOR and (d) water cut.

**Square Root of Time Plot.** A common question that arises in this context, is how the combined effect of superposition and multiphase flow impacts the square root of time plot. For this example, the square root of time plot for all the evaluated OOIPs are provided in **Fig 12**. One can see that the classic diagnostic plot, even in this simple multiphase flow example, behaves highly non-linear, even during infinite acting flow.

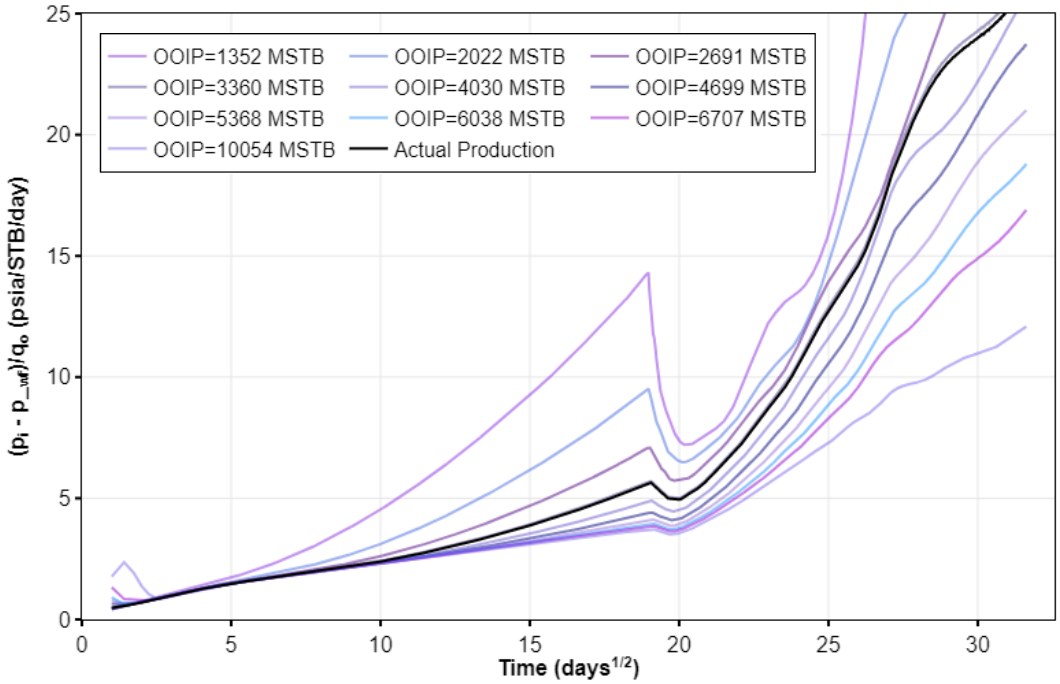


Fig 12— The square root of time plot for different the OOIP analyzed in this example.

## Numerically Assisted RTA: Field-Data Example

For a field example, it is helpful to split the workflow into three parts:

1. Define a relevant fluid initialization and relative permeability.
2. Pick a representative LFP' and OOIP.
3. Resolve parameters for history matching ($x_f$ and $k$).

These three steps manifest one of the key benefits of the proposed workflow, i.e., the decoupling of multiphase flow related data (PVT, initial saturations and relative permeabilities) from well geometry and petrophysical properties ($L$, $x_f$, $h$, $n_f$, $\varphi$, $k$).

**1. Fluid initialization, relative permeability**

When applying the numerical RTA workflow on field data, it is important to consider the uncertainty in the input and assumptions going into the analysis.

a) A key input is the actual bottomhole (sandface) pressures versus time. If these pressures are measured and properly converted from gauge depth to sandface (if relevant), the uncertainty in this input is low. However, if these pressures are calculated from readily available surface data (surface pressures, production rates and well configuration), a potential source of uncertainty is introduced.

b) The method assumes a reservoir representative fluid initialization, which includes correct initial conditions ($p_{Ri}| T_R$), PVT properties ($B_o, R_s, \mu_o \mid B_{gd}, r_s, \mu_g$) and saturations ($S_{wi}, S_{oi}, S_{gi}$). To reduce uncertainty in the fluid model itself, it is recommended to create PVT tables from an equation of state (EOS) model tuned to all the available and measured PVT data in the relevant field/basin (Younus et al. 2019).

c) The methodology assumes a representative relative permeability set. Compared to bottomhole pressures and PVT, there is a lack of available relative permeability measurements performed on tight unconventional rocks. Hence, a default set (e.g., Corey) is typically applied and only changed if necessary to match historical data.

One might argue that a weakness of the numerical RTA methodology is that it is dependent on all the aforementioned assumptions. However, all reservoir engineering analysis have either explicit, or implicit assumptions of both pressure, PVT and relative permeability. Take decline curve analysis (DCA) as the simplest example. First, DCA has an inherent assumption of pressure, i.e., it assumes a constant bottomhole pressure ($p_{wf}$ = constant). In addition, when DCA is performed on both the oil and gas phase of a well, an implicit producing GOR profile is also assumed. Point being that the producing GOR[10], $R_p$, is just a composite result of PVT and relative permeability, as given by Fetkovich (1986) in **Eq. 6**:

$$R_p = \left[1 + \frac{k_{rg} B_o \mu_o}{k_{ro} B_{gd} \mu_g} r_s\right]^{-1} \left[R_s + \frac{k_{rg} B_o \mu_o}{k_{ro} B_{gd} \mu_g}\right] \quad (6)$$

In a practical context, one can ensure that a provided fluid initialization and relative permeability set is reasonable by running the "infinite acting" case (step 1) a few times before moving on to the LFP' and OOIP interpretation. This is mainly ensuring that the relative rates (GORs and water cuts) make sense, before generating the different type curves (next step). In short, it is important to alter the PVT, initial water saturation and relative permeability to ensure that the:

i. simulated producing GOR from the infinite acting case should be equal to or less than the actual GOR. The GOR of the infinite acting model should never be higher than the actual GOR. If a

[10]Other associated equations are provided in Appendix A: Cheat Sheet for Engineers.

mismatch between actual GOR and the simulated IA GOR is observed (higher than the simulated GOR), this likely indicates departure from IA linear flow.

ii. mismatch between the observed water cut and the simulated water cut is as small as possible. Some mismatch during the early time (during flowback) is expected. Water cut is not very sensitive to flow regime so one should not expect a major change in water cut after reaching end of infinite acting behavior.

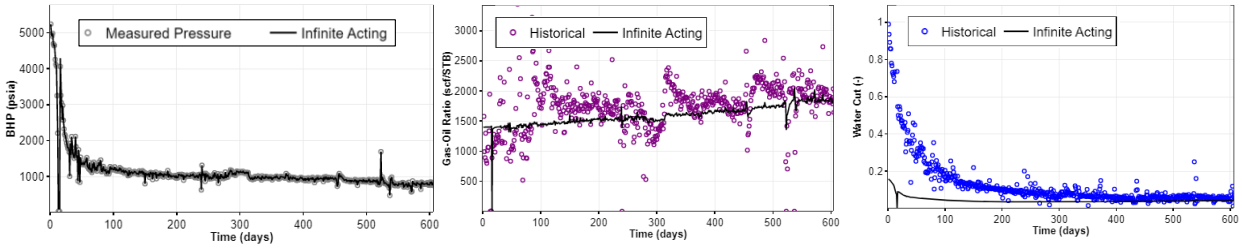


Fig 13—Example of consistent GOR behavior (equal or lower than observed) and water cut behavior (focus on stabilized water cut) late time.

After altering PVT, initial water saturation and relative permeability, the relative rates performance versus time, for both the historical data and the infinite acting model, could for instance look like the example provided in **Fig 13.** The associated fluid initialization (PVT and initial saturations) and relative permeability is provided in **Table 2.**

Table 2—Fluid initialization and relative permeability for real case.

| | | | | | | | | |
|---|---|---|---|---|---|---|---|---|
| $p_{Ri}$ | 5500 | psia | $F_{CD}$ | 8 | - | $n_{w,}$ $n_{ow}$ | 1.8 | - |
| $T_R$ | 186 | F | $S_{wi}$, $S_{gi}$, $S_{orw}$ | 20 | % | $n_g$ | 1.5 | - |
| $R_{si}$ | 1400 | scf/STB | $S_{wc}$ | 10 | % | $n_{og}$ | 4 | - |
| $B_o$ | 1.694 | RB/STB | $S_{gc}$ | 5 | % | $k_{rocw}$, $k_{rwro}$, $k_{rgro}$ | 1 | - |

## 2. Select LFP' and OOIP.

With a reasonable fluid initialization and relative permeability set, the numerical RTA workflow (steps 1-8) can be performed. **Fig. 14** provides both the cumulative and instantaneous LFP' plots, both indicating that the LFP' is around 45,000 $ft^2md^{1/2}$. Interestingly, the well is still behaving infinite acting after around 600 days, hence picking the OOIP = 4491 MSTB would be a conservative (lower limit) case as it is still unknown "how large the tank is".

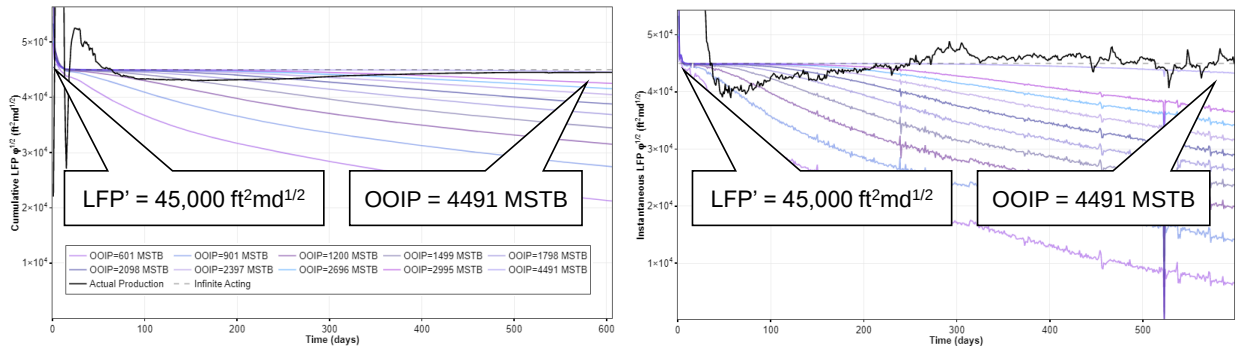


Fig. 14— LFP' plots for field data, both "cumulative LFP" and "instantaneous LFP".

In a perfect world, all the diagnostic plots should line up and indicate the same LFP' and OOIP. However, this is more challenging when working with real data, both subject to noise and uncertainty. For this example, the LFP' and OOIP picked in Fig. 14 provide the different, associated diagnostic plots presented in **Fig. 15**. As observed in Fig. 15a, the cumulative oil plot indicates excellent alignment with the picked LFP' and OOIP. The cumulative gas curve in Fig. 15b is somewhat harder to draw a conclusion from, as

all the type curves collapse to almost the same cumulative gas curve. This is observed for some lower GOR oils and is a result of a decrease in well productivity being compensated by the increase in GOR from a smaller OOIP case (tank) being more depleted. Hence, using the producing GOR behavior actively, as observed in Fig. 15c, more confidence is gained in that the picked OOIP is reasonable. Lastly, as observed in Fig. 15d, the water cut plot mismatch for the early time data is significant, which is a period mainly dominated by flowback water. Consistently accounting for completion water in the numerical RTA workflow is beyond the scope of this paper but is an important item for further investigation. That said, one can clearly observe the relative *insensitivity* to flow regime that water cut performance has compared to producing GOR, especially considering the natural noise in the water production data, and complications of dealing with both stimulation and formation water.

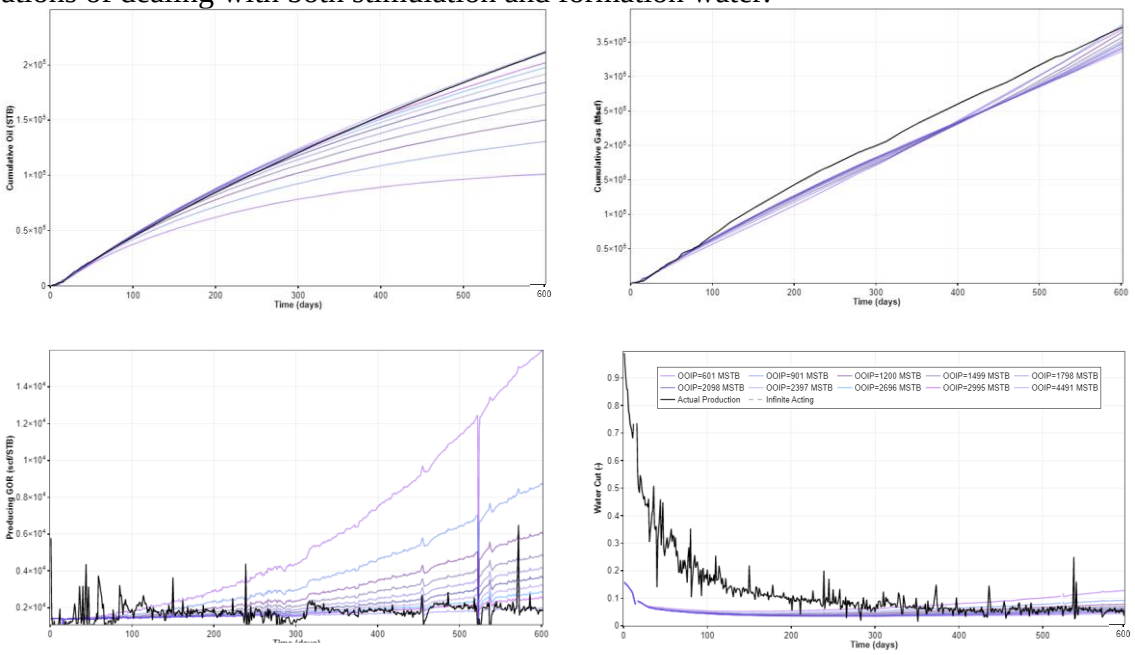


Fig. 15—. (a) cumulative oil, (b) cumulative gas, (c) producing GOR and (d) producing water cut

### 3. Resolve parameters for history matching.

To use the numerical RTA outputs in a history matching exercise, key parameters such as $k$ and $x_f$ must be resolved from Eqs. 4-5 to ensure consistent results. In this example, $L = 7500\ ft$, $h = 150\ ft$, $n_f = 100$ and $\varphi = 5\%$, will result in a $k$ ~ 50 nd and $x_f$ ~ 472 ft. By importing these parameters into a history matching exercise, in which the resolved parameters are used by default, the first run generates the results presented in **Fig. 16**. Note that the model is controlled on bottomhole pressure. Additional, minor adjustments can be included to get an even better history match. This is a good example of how the systematic workflow outlined in this paper can be used to quickly obtain, rigorous and accurate physics-based results. A consistent conversion of the $F_{cd}$ parameter used in the numerical RTA workflow, provided in Table 2, to what is used in the history matching exercise has been applied.

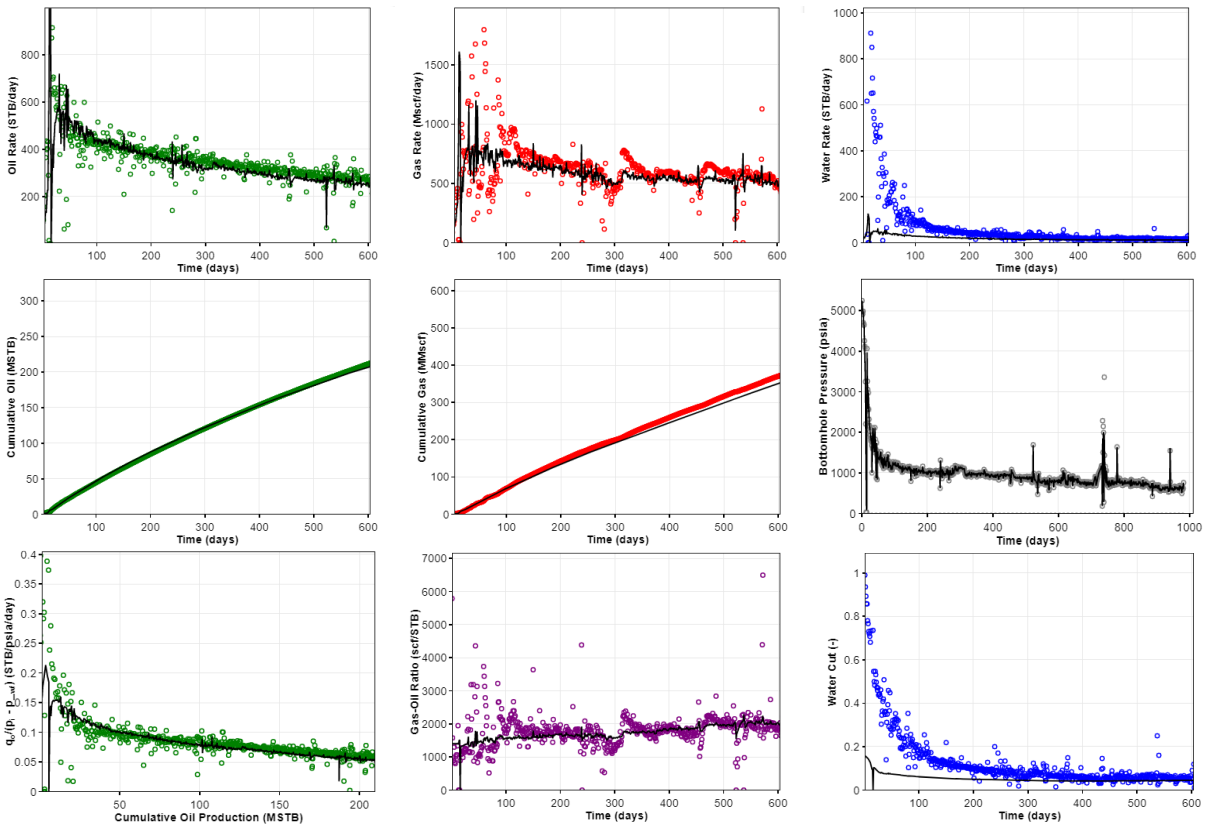


Fig. 16—First run realization using output from history matching exercise.

## Finite Conductivity Fractures – Low Dimensionless Fracture Conductivity ($F_{cd}$)

Sometimes an additional pressure drop in the fracture might be required to match historical observed data (e.g., GOR performance), and this can be included in the model by assigning a low dimensionless fracture conductivity ($F_{cd}$) to the model at hand. The case presented in the last section, with properties presented in Table 2, is an example of that. The lower the $F_{cd}$, the higher the pressure drop in the fracture. A finite conductivity fracture may be associated with a "linear GOR increase" when the flowing bottomhole pressure is below the saturation pressure.

The physical reasons for this additional pressure drop can be many, but numerically a low $F_{cd}$ will add extra pressure drop between the reservoir and the well. Wells that exhibit this behavior might qualify as clean-up candidates. To consistently incorporate a finite conductivity fracture into the numerically assisted RTA workflow, one needs to know how the definition of $F_{cd}$ changes when other parameters change (e.g., permeability, height, number of fractures).

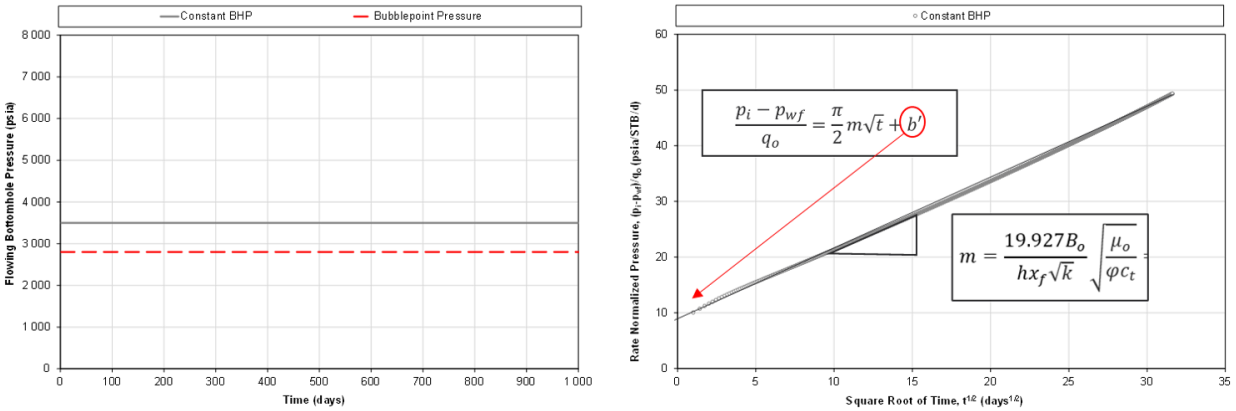


Fig. 17—Example of square root of time plot for finite conductive fracture.

For an ideal model (i.e., single-phase flow, controlled on a constant bottomhole pressure), infinite acting, linear flow associated with flow through a finite conductive fracture manifests itself as a positive intercept on the square root of time plot, as exemplified in **Fig. 17.**

For a well with a given slope ***m***, which is a product of LFP' and PVT related parameters, the intercept should be the same no matter what combination of parameters that make up ***m***, i.e., irrespective of LFP'. Hence, given the relationships presented in **Eqs. 7-9**,

$$\frac{p_i - p_{wf}}{q_o} = \frac{\pi}{2} m\sqrt{t} + b' \tag{7}$$

$$F_{cd} = \frac{141.2 B \mu}{b'(p_i - p_{wf}) k\, h\, n_f}\, \beta \tag{8}$$

$$\beta = \left(1 + \frac{h}{x_f}\left(\ln\left(\frac{h}{2r_w}\right) - \frac{\pi}{2}\right)\right) \tag{9}$$

one can convert $F_{cd}$ consistently with

$$F_{cd,2} = F_{cd,1} \frac{k_1 h_1 n_{f,1}}{k_2 h_2 n_{f,2}} \frac{\beta_2}{\beta_1} \tag{10}$$

For the field example provided in the last section, the $F_{cd,1} = 8$ used in the numerical RTA workflow is converted consistently with Equation 10 to $F_{cd,2} = 14$ used in the history matching realization presented in Fig. 16. The conversion must be performed based on the parameters used in the "template model" (step 1). Relevant for this conversion are the following parameters used in the "template model": $r_{w,1} = 1\, ft$, $x_{f,1} = 400\, ft$, $h_1 = 200\, ft$, $N_{f,1} = 1$ and $k_1 = 200\, nd$.

## Correlating Numerical RTA output to Completion Metrics

When performing the analysis across wells with very different fluid initializations, it is not fair to only correlate the completion data to OOIP. To illustrate, let us assume a reservoir with only water ($S_{wi} = 100\%$). No matter how much fracture/surface area the completion created, the OOIP will always be 0. Hence, to quantify the completion effectiveness in an isolated manner, irrespective of fluid type, it would be fair to correlate this to the contacted pore volume, $V_p$, which can be easily calculated from OOIP as given in **Eq. 11**.

$$V_p = \frac{HCPV}{1 - S_{wi}} = \left(\frac{OOIP}{1 - S_{wi}}\right) B_{ti} \tag{11}$$

Taking this one step forward, the gross rock volume contacted, $V_R$, can easily be calculated with **Eq. 12**, to also account for changes in porosity across the wells analyzed.

$$V_R = \frac{V_p}{\varphi} \tag{12}$$

## Dry Gas Wells

For dry gas wells, there is no OOIP ($B_{ti} = \infty$). Hence, OGIP must be resolved instead of OOIP in the numerical RTA workflow. The formula for OGIP is given in **Eq. 13**.

$$OGIP = \frac{2x_f Lh\varphi(1 - S_{wi})}{B_{gd}} \tag{13}$$

## Template Model

The numerical RTA workflow requires a "base" numerical model to be run systematically, the "template model". In theory, the properties of this "template model" can be arbitrary, i.e., it does not matter what permeability, height, number of fractures, porosity and lateral length that is used, as long as one follows the general steps of the workflow. In practice, however, there might be numerical reasons for picking a certain "template model", as some pairs of parameters have better performance from a numerical perspective (convergence, speed, stability). Finding the optimal template model is beyond the scope of this paper, but for the sake of completeness, the template model used in this paper is provided below in **Table 3.**

Table 3—Default parameters in template model.

| | | | | | | | | | | | |
|---|---|---|---|---|---|---|---|---|---|---|---|
| $L_w$ | 150 | ft | $x_e$ | 400 | ft | $h_f$ | 200 | ft | k | 200 | nd |
| $n_f$ | 1 | - | $x_f$ | 400 | ft | h | 200 | ft | φ | 0.05 | - |

## Future Work

Although the numerical RTA workflow has already shown promise, it is important to remember that the methodology is still in its infancy. After using the methodology for a wide range of wells in North-American unconventionals, the authors have identified the following areas for future work.

- Investigate whether it is possible to consistently account for completion water in the methodology. In most wells, an early time discrepancy between simulated water cut and observed water cut is observed, as the frac water is not accounted for in the model.
- Study how i) well interference, ii) non-ideal well geometries, iii) differential depletion and iv) relative permeability assumptions impact the analysis.

- Assess whether the gridding and the physical parameters assigned to the "template model" can be optimized for increased performance from both a numerical (convergence) and computational (speed) perspective.
- Evaluate if shut-in periods, and their associated pressure build-ups, can be used to further constrain the results from numerical RTA. This may also enable better calibration of inputs such as $F_{cd}$ (low $F_{cd}$ rapid build-up, high $F_{cd}$ slow build-up).
- Try performing the numerical RTA method simultaneously for several wells, rather than for each individual well, while minimizing the error of the whole set. Uncertain input parameters such as relative permeability could be assigned to the whole group of wells and changed in tandem to minimize the overall error.
- Attempt to include more complex "base models" than the 1D symmetry of element model used in this paper. Although the simplicity of the base model has significant advantages, alterations to the base model to include other models like a stimulated region around the fracture (enhanced fracture region) can be applied.

## Summary

To summarize, the numerical RTA workflow outlined in this paper:

- Is readily applied and offers repeatability, such that many wells can be analyzed efficiently.
- Solves the inherent problems associated with rigorous superposition and multiphase flow effects, involving time and spatial changes in pressure, compositions and PVT properties, saturations and complex phase mobilities.
- Decouples multiphase flow data (PVT, initial saturations and relative permeabilities) from well geometry and petrophysical properties, providing a rigorous yet rapid and semi-automated approach to define production performance for many wells.
- Does not require semi-analytical models, time and spatial superposition (convolution), pseudo pressure and pseudo time transforms. Avoiding a long list of complex analytical equations makes the methodology easier to verify in the technical community and makes the methodology more susceptible to adoption.
- Utilizes a full-physics numerical model, which makes it a trivial exercise to export the results from RTA analysis into higher order analysis, such as a full-physics reservoir and associated history matching.
- The method has proven to increase the consistency between engineers in a team compared to traditional RTA methods (URTeC 2967)

## Nomenclature

$b$ = rate exponent

$B_{gd}$ = "dry" Gas Formation Volume Factor

$B_o$ = oil formation volume factor

$B_t$ = total formation volume factor

$c_g$ = gas compressibility

$c_o$ = oil compressibility

$c_r$ = rock compressibility

$c_t$ = total compressibility

$c_w$ = water compressibility

$D_i$ = nominal decline rate at time zero

$F_{cd}$ = dimensionless fracture conductivity

$h$ = height

$h_f$ = fractured height

$L$ = well length

m = slope on "square-root-of-time" plot

$n_f$ = number of fractures

$N$ = cumulative production

$k$ = matrix permeability

$k_{rp}$ = relative permeability of phase p

$p_i$ = initial reservoir pressure

$p_{sat}$ = saturation pressure

$p_{wf}$ = flowing bottomhole pressure

$q_i$ = initial flow rate

$q_{\bar{g}o}$ = surface gas rate from res. oil phase

$q_{\bar{o}o}$ = surface oil rate from res. oil phase

$q_{\bar{g}g}$ = surface gas rate from res. gas phase

$q_{\bar{o}g}$ = surface oil rate from res. gas phase

$q_o$ = reservoir gas rate

$q_g$ = reservoir gas rate

$q_w$ = water rate

$r_s = R_v$ = solution CGR = vaporized oil ratio

$r_w$ = well radius

$R_p$ = producing GOR

$R_s$ = solution GOR

$S_{gi}$ = initial gas saturation

$S_{oi}$ = initial oil saturation

$S_{wi}$ = initial water saturation

$t$ = time

$V_p$ = pore volume

$V_R$ = gross rock volume

$x_f$ = fracture half length

$x_e$ = reservoir half extent

$\mu$ = viscosity

$\varphi$ = porosity

$\rho$ = density

## Acknowledgments

This paper is dedicated to Michael J. “Mike” Fetkovich, a pioneer in rate transient analysis that passed away in 2020. His contributions to the industry will never be forgotten. We would also like to thank Innovation Norway and the Norwegian Research Council for supporting our research on this topic.

## References

Agarwal, R. G. Real Gas Pseudo-Time" - A New Function For Pressure Buildup Analysis Of MHF Gas Wells." Paper presented at the SPE Annual Technical Conference and Exhibition, Las Vegas, Nevada, September 1979. doi: https://doi.org/10.2118/8279-MS

Bowie, B., and Ewert, J. (2020, July 20). Numerically Enhanced RTA Workflow - Improving Estimation of Both Linear Flow Parameter And Hydrocarbons In Place. Unconventional Resources Technology Conference. doi:10.15530/urtec-2020-2967

Carslaw, H. S. and Jaeger, J. C. 1959. Conduction of Heat in Solids. Oxford, UK: Clarendon Press.

Clarkson, C. R., et al. 2019. Anomalous Diffusion or Classical Diffusion in an Anomalous Reservoir? Evaluation of the Impact of Multiphase Flow on Reservoir Signatures in Unconventional Reservoirs, Denver, Colorado, 22-24 April. URTeC 85

Fetkovich, M. J. (1973, January 1). Decline Curve Analysis Using Type Curves. Society of Petroleum Engineers. doi:10.2118/4629-MS

Fetkovich, M.D., Guerrero, E.T., Fetkovich, M.J., and L.K. Thomas. "Oil and Gas Relative Permeabilities Determined From Rate-Time Performance Data." Paper presented at the SPE Annual Technical Conference and Exhibition, New Orleans, Louisiana, October 1986. doi: https://doi.org/10.2118/15431-MS

Fevang, Ø, and Whitson, C.H. "Modeling Gas-Condensate Well Deliverability." SPE Res Eng 11 (1996): 221–230. doi: https://doi.org/10.2118/30714-PA

Jones, J.R. 1986. "Computation and analysis of single well responses for gas condensate systems". PhD dissertation, University of Tulsa.

Jones, R. S. "Producing-Gas/Oil-Ratio Behavior of Multifractured Horizontal Wells in Tight Oil Reservoirs." SPE Res Eval & Eng 20 (2017): 589–601. doi: https://doi.org/10.2118/184397-PA Kazemi, H., Eker, I., Torcuk, A. M., & Kurtoglu, B. (2015, October 10). Fundamentals of Gas Shale Reservoirs. Published 2015 by John Wiley & Sons, Inc.

Miller, F. G. 1962. Theory of Unsteady-State Influx of Water in Linear Reservoirs. J. Inst. Petrol. 48 (467): 365-379

Wattenbarger, R. A., El-Banbi, A. H., Villegas, M. E., & Maggard, J. B. (1998, January 1). Production Analysis of Linear Flow Into Fractured Tight Gas Wells. Society of Petroleum Engineers. doi:10.2118/39931-MS

Whitson, C. H., Coll, C., Dahouk, M. M., & Juell, A. O. (2016, May 30). Shale Reserve Forecasting - Model Consistency and Uncertainty. Society of Petroleum Engineers. doi:10.2118/180140-MS

# Appendix A: Cheat Sheet for Engineers

## Decline Curve Analysis (DCA)

### Arps

$q(t) = q_i(1 + bD_it)^{-\frac{1}{b}}$ , …… (A1)

| ***b* value** | **Scenario** |
|---|---|
| 0 | Single-phase liquid |
| 0.1-0.4 | Solution gas drive reservoirs |
| 0.4-0.5 | Single phase gas |
| 0.5-1.0 | Layered reservoirs |
| >=1 | Infinite acting reservoirs |

### Exponential Decline (b=0)

$q = q_i e^{-D_i t}$, …… (A2)

$N(t) = \frac{q_i}{D_i}(1 - e^{-D_i t})$, …… (A3)

$N(\infty) = \frac{q_i}{D_i}$, …… (A4)

### Hyperbolic (0 < b < 1)

$q = q_i(1 + bD_it)^{-\frac{1}{b}}$, …… (A5)

$N(t) = \frac{q_i}{(b-1)D_i}(1 - e^{-D_i t})\left[(1 + bD_it)^{1-\frac{1}{b}} - 1\right]$, . (A6)

$N(\infty) = \frac{q_i}{D_i}\left(\frac{1}{1-b}\right)$, …… (A7)

### Harmonic (b = 1)

$q = q_i(1 + D_it)^{-1}$, …… (A8)

$N(t) = \frac{q_i}{D_i}\ln(1 + D_it)$, …… (A9)

$N(\infty) = \infty$, …… (A10)

### Harmonic (b >= 1)

$q = q_i(1 + bD_it)^{-\frac{1}{b}}$, …… (A11)

$N(t) = \frac{q_i}{(b-1)D_i}(1 - e^{-D_i t})\left[(1 + bD_it)^{1-\frac{1}{b}} - 1\right]$,(A12)

$N(\infty) = \infty$, …… (A13)

## Numerical RTA

$LFP = 4n_f x_f h\sqrt{k}$, …… (A14)

$LFP' = LFP\sqrt{\varphi} = 4n_f x_f h\sqrt{k}\sqrt{\varphi}$ , …… (A15)

$OOIP = \frac{2x_f Lh\varphi(1-S_{wi})}{B_t}$, …… (A16)

$LFP\sqrt{\varphi}/OOIP = \frac{2n_f\sqrt{k}}{L\sqrt{\varphi}(1-S_{wi})}B_t$ , …… (A17)

$k = \left[\frac{(LFP\sqrt{\varphi}/OOIP)(1-S_{wi})\sqrt{\varphi}L}{2B_t n_f}\right]^2$ , …… (A18)

$x_f = \frac{LFP}{4n_f h\sqrt{k}}$, …… (A19)

$B_t = \frac{S_o+S_g}{\frac{S_o}{B_o}+\frac{S_g}{B_{gd}/r_s}}$, …… (A20)

$V_p = \frac{HCPV}{1-S_{wi}} = \left(\frac{OOIP}{1-S_{wi}}\right)B_{ti}$ , …… (A21)

$V_t = V_p/\varphi$ , …… (A22)

$OGIP = \frac{2x_f Lh\varphi(1-S_{wi})}{B_{gd}}$ , …… (A23)

## Producing GOR & $k_{rg}/k_{ro}$

$R_p = [1 + \alpha r_s]^{-1}[R_s + \alpha]$ , …… (A24)

$\alpha = \frac{k_{rg}B_o\mu_o}{k_{ro}B_{gd}\mu_g}$ , …… (A25)

For $r_s = 0$,

$R_p = \frac{q_w}{q_{\bar{o}g}+q_{\bar{o}o}} = R_s + \frac{k_{rg}B_o\mu_o}{k_{ro}B_{gd}\mu_g}$, …… (A26)

Solve for $k_{rg}/k_{ro}$

$\frac{k_{rg}}{k_{ro}} = \frac{R_p-R_s}{1-R_p r_s}\frac{B_{gd}\mu_g}{B_o\mu_o}$ , …… (A27)

## Analytical Rate Transient Analysis

**Infinite Conductivity**

$$m = \frac{19.927 B_o}{h x_f \sqrt{k}} \sqrt{\frac{\mu_o}{\varphi c_t}} = \frac{79.708 B_o}{4 h x_f \sqrt{k}} \sqrt{\frac{\mu_o}{\varphi c_t}} \text{ , ..... (A28)}$$

$$m = \frac{79.708 B_o}{LFP\sqrt{\varphi}} \sqrt{\frac{\mu_o}{c_t}} = \frac{79.708 B_o}{LFP'} \sqrt{\frac{\mu_o}{c_t}} \text{ , ..... (A29)}$$

Constant flowing pressure

$$\frac{p_i - p_{wf}}{q_o} = \frac{\pi}{2} m \sqrt{t} \text{ , ..... (A30)}$$

Constant rate solution

$$\frac{p_i - p_{wf}}{q_o} = m \sqrt{t} \text{ , ..... (A31)}$$

**Finite Conductivity**

$$\frac{p_i - p_{wf}}{q_o} = \frac{\pi}{2} m \sqrt{t} + b' \text{ , ..... (A32)}$$

$$F_{cd} = \frac{141.2 B \mu}{b'(p_i - p_{wf}) k\, h\, n_f} \beta \text{ , ..... (A33)}$$

$$\beta = \left(1 + \frac{h}{x_f}\left(\ln\left(\frac{h}{2 r_w}\right) - \frac{\pi}{2}\right)\right) \text{ , ..... (A34)}$$

Changing $F_{cd}$ when other parameters are changed:

$$F_{cd,2} = F_{cd,1} \frac{k_1 h_1 n_{f,1}}{k_2 h_2 n_{f,2}} \frac{\beta_2}{\beta_1} \text{ , ..... (A35)}$$

## Darcy

$$\overrightarrow{v_o} = -\frac{k k_{ro}}{\mu_o} \nabla(p_o + \rho_o g h) \text{ , ..... (A36)}$$

$$\overrightarrow{v_g} = -\frac{k k_{rg}}{\mu_g} \nabla\left(p_g + \rho_g g h\right) \text{ , ..... (A37)}$$

$$\overrightarrow{v_w} = -\frac{k k_{rw}}{\mu_w} \nabla(p_w + \rho_w g h) \text{ , ..... (A38)}$$

## Producing Water Cut

For oils ($r_s = 0$)

$$\frac{1}{WC} = \frac{q_w + q_{\bar{o}o}}{q_w} = 1 + \frac{k_{ro} B_w \mu_w}{k_{rw} B_o \mu_o} \text{ , ..... (A39)}$$

$$\frac{k_{rw}}{k_{ro}} = \frac{B_w \mu_w}{B_o \mu_o}\left(\frac{WC}{1 - WC}\right) \text{ , ..... (A40)}$$

For gas condensates / wet gases ($r_s > 0$ & $k_{ro} = 0$)

$$\frac{1}{WC} = \frac{q_w + q_{\bar{o}g}}{q_w} = 1 + \frac{k_{rg} \mu_w B_w r_s}{k_{rw} \mu_g B_{gd}} \text{ , ..... (A41)}$$

$$\frac{k_{rw}}{k_{rg}} = \frac{\mu_w B_w r_s}{\mu_g B_{gd}}\left(\frac{WC}{1 - WC}\right) \text{ , ..... (A42)}$$

## Other Useful Equations

**Total Compressibility**

$$c_t = c_r + S_o c_o + S_w c_w + S_g c_g \text{ , ..... (A43)}$$

**Isothermal Compressibility**

$$c = -\frac{1}{V}\left(\frac{\partial V}{\partial p}\right)_T = \frac{1}{\rho}\left(\frac{\partial \rho}{\partial p}\right)_T = \frac{1}{B}\left(\frac{\partial B}{\partial p}\right)_T \text{ , ..... (A44)}$$

**Superposition (Linear) Time**

$$t_n = \left(\sum_{j=1}^{n} \frac{q_j - q_{j-1}}{q_n} \sqrt{t - t_{j-1}}\right)^2 \text{ , ..... (A45)}$$

**Material Balance Time**

$$t_n = \frac{Q_n}{q_n} \text{ , ..... (A46)}$$

**Diffusivity Equation (radial coordinates)**

$$\partial^2 p / \partial r^2 + r^{-1} \partial p / \partial r = \eta^{-1} \partial p / \partial t \text{ , ..... (A47)}$$

$$\eta = k / \varphi \mu c \text{ , ..... (A48)}$$

## Appendix B: Providing Physical Significance to DCA Parameters

DCA parameters, i.e., $q_i$, $D_i$ and $b$, represent underlying, physical parameters. To convince ourselves that this is the case, a single-phase oil well, producing at a constant bottomhole pressure is analyzed. The well is an idealized multi-fractured horizontal well (MFHW), as exemplified in Fig. 1, with negligible production beyond the fracture tips. Linear flow is perpendicular to the fractures. For such a model, there will first be a period of infinite acting flow (IAF). The duration of this period depends on parameters such as permeability and distance to the closest offset fracture. Boundary-dominated flow (BDF) occurs after pressure at the no-flow boundary between fractures declines to less than the initial reservoir pressure. For such a case, the generalized Arps equation **Eq. B1** can be tied to the analytical solutions for both infinite acting and boundary dominated flow periods as presented in **Eqs. B2-B8**.

$$q(t) = q_i(1 + bD_i t)^{-\frac{1}{b}}, \quad \text{(B1)}$$

$$q_i = \begin{cases} \frac{hx_f\sqrt{k}}{31.3B_o}\sqrt{\frac{\varphi c_t}{\mu_o}}p_i - p_{wf} = \frac{LFP\sqrt{\varphi}}{125.2B_o}\sqrt{\frac{c_t}{\mu_o}}p_i - p_{wf}, & t_{elf} < 0 \\ \frac{4hx_f k}{141.2B_o}\frac{p_i - p_{wf}}{\mu_o \pi y_e} = \frac{LFP\sqrt{k}}{141.2B_o}\frac{p_i - p_{wf}}{\mu_o \pi y_e}, & t_{elf} \geq 0 \end{cases}, \quad \text{(B2)}$$

$$D_i(t) = \begin{cases} \frac{1}{2}, & t < t_{elf} \\ \frac{\pi^2}{4}\frac{0.00633k}{y_e^2 \varphi c_t \mu_o}, & t \geq t_{elf} \end{cases}, \quad \text{(B3)}$$

$$b(t) = \begin{cases} 2, & t < t_{elf} \\ 0, & t \geq t_{elf} \end{cases}, \quad \text{(B4)}$$

$$t_{elf} = \frac{y_e^2 \mu \phi c_t}{0.159k}, \quad \text{(B5)}$$

$$Q(t) = \int_0^{\infty} q(t)\, dt, \quad \text{(B6)}$$

$$Q(\infty) = \int_0^{t_{elf}} q_{IA}\, dt + \int_{t_{elf}}^{\infty} q_{BDF}\, dt, \quad \text{(B7)}$$

$$Q(\infty) = \left(2q_i\left[\left(t_{elf} + 1\right)^{\frac{1}{2}} - 1\right]\right)_{IA} + \left(\frac{q_i}{D_i}e^{-D_i t_{elf}}\right)_{BDF}, \quad \text{(B8)}$$

The verification of the results with a numerical simulator is provided in Fig 18, with associated, physical parameters provided in **Table 4**. As observed, all the curves overlay. A question that arises in this context is whether the PVT properties should be evaluated at (1) the initial reservoir pressure, (2) the flowing bottomhole pressure (constant in this case), or (3) some average pressure. Agarwal (1979) introduces the concept of *pseudotime* to solve this issue in an accurate manner. However, for the purposes of this example, evaluating the PVT dependent properties ($B_o$, $\mu_o$, $c_t$) at the midpoint of initial reservoir pressure and the flowing bottomhole pressure provides satisfactory results, i.e., $p = (p_i + p_{wf})/2$. From this very simple case, the following conclusions can be made: (i) as originally shown by Fetkovich in 1973, the Arps parameters ($q_i$, $D_i$ and $b$) represent underlying physical parameters and (ii) $b$ and $D_i$ values vary used to describe infinite acting behavior will often vary with time.

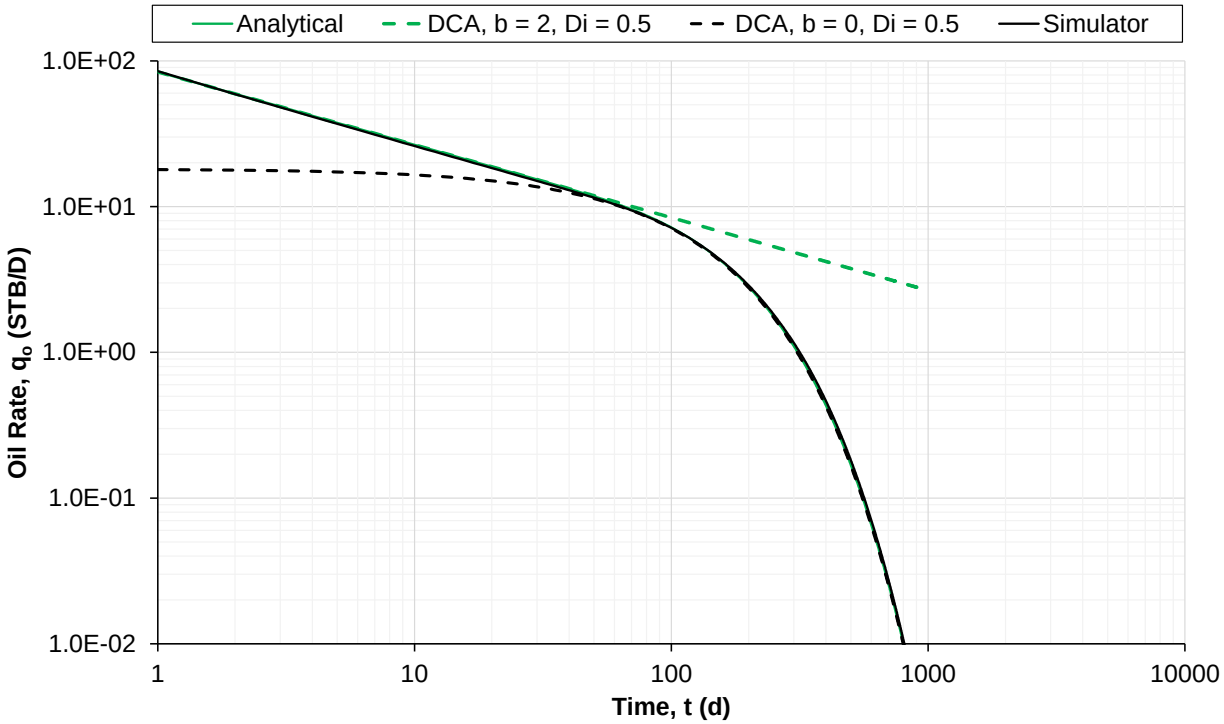


Fig 18—Comparison of results DCA (with parameters from physical analytical equations) and a full-physics reservoir simulator.

Table 4. Relevant parameters for the results presented in Fig 18.

| Analytical Parameters | | |
|---|---|---|
| | **Field Units** | **SI Units** |
| **$\mu$** | 0.624 cp | 0.000624 Pa s |
| **$\varphi$** | 0.05 | 0.05 |
| **$c_r$** | 4.000E-06 1/psi | 5.80E-10 1/Pa |
| **$c_w$** | 3.000E-06 1/psi | 4.35E-10 1/Pa |
| **$c_o$** | 1.330E-05 1/psi | 1.93E-09 1/Pa |
| **$c_t$** | 1.730E-05 1/psi | 2.51E-09 1/Pa |
| **$k_m$** | 2.000E-04 md | 1.97E-19 m2 |
| **$y_e$** | 25 ft | 7.62 m |
| **$p_i$** | 7500 psia | 51725700 Pa |
| **$p_{wf}$** | 2500 psia | 17241900 Pa |
| **$x_f$** | 500 ft | 152.40 m |
| **$h_f$** | 150 ft | 45.72 m |
| **$B_o$** | 1.196 RB/STB | 1.196 RB/STB |

To provide physical significance to the DCA parameters b, $D_i$ and $q_i$, the analytical solutions for both infinite acting linear flow and boundary dominated flow must be written on the form of Arps. To do this, the following assumptions are applied: (1) constant bottomhole pressure, (2) single-phase oil flow and (3) no volume beyond the frac tip and (4) one homogenous layer. This results in so-called "1D flow", with transition directly from infinite acting linear flow to boundary dominated flow at $t_{elf}$.

**Linear Flow.** The analytical equation for constant pressure is (Wattenbarger, 1998)

$$q_o = \frac{hx_f\sqrt{k}}{31.3B_o}\sqrt{\frac{\varphi c_t}{\mu_o}}(p_i - p_{wf})t^{-\frac{1}{2}}, \quad \text{(B9)}$$

One immediate observation is that q(t=0) in Arps and q(t=0) in the analytical equation yield inconsistent results, i.e., $q_{o,DCA}(t=0) = q_i$, while $q_{o,RTA}(t=0) = 0$. Substitution, in which $t = t_0 + 1$, where $t_0$ = 0, 1, 2, 3, etc., yield,

$$q_o = \frac{hx_f\sqrt{k}}{31.3B_o}\sqrt{\frac{\varphi c_t}{\mu_o}}\left(p_i - p_{wf}\right)(1+t_o)^{-\frac{1}{2}}, \quad \text{(B10)}$$

which can be written on the form $q_i(1+bD_it)^{-\frac{1}{b}}$, where $q_i = \frac{hx_f\sqrt{k}}{31.3B_o}\sqrt{\frac{\varphi c_t}{\mu_o}}(p_i - p_{wf})$, $b = 2$ and $D_i = \frac{1}{2}$.

**Boundary Dominated Flow.** The analytical solution for constant pressure is (Carslaw and Jaeger, 1959; Miller, 1962)

$$q_o = \frac{4x_fhk(p_i-p_{wf})}{141.2B_o\mu_o\pi y_e}\sum_{n_{odd}}^{\infty} e^{-n^2\frac{\pi^2}{4}\frac{0.00633k}{y_e^2\mu_oc_t}t} \approx \frac{4x_fhk(p_i-p_{wf})}{141.2B_o\mu_o\pi y_e}e^{-\frac{\pi^2}{4}\frac{0.00633k}{y_e^2\mu_oc_t}t}, \quad \text{(B11)}$$

Which can be rewritten on the form $q = q_ie^{-D_it}$, where $q_i = \frac{4x_fhk(p_i-p_{wf})}{141.2B_o\mu_o\pi y_e}$, $b = 0$ and $D_i = \frac{\pi^2}{4}\frac{0.00633k}{y_e^2\mu_oc_t}$.

**Time to end of linear flow.** The analytical solution given in **Eq. B5** for time to end of linear flow is given by Wattenbarger (1998).

## Appendix C: Flow Regimes Summary

**Infinite acting flow ($\frac{\partial p}{\partial t} \neq constant$):** is often referred to as transient flow, or sometimes unsteady flow. This flow regime ends as the pressure transient reaches *one* reservoir boundary.

**Transitional flow:** This flow regime starts as the pressure transient reaches *one* reservoir boundary and ends when the pressure propagation reaches *all* reservoir boundaries.

**Boundary dominated flow ($\frac{\partial p}{\partial t} = constant$):** This flow regime starts as the pressure propagation reaches *all* reservoir boundaries.

i. Pseudo-steady state (PSS). Occurs when *all* outer boundaries of the reservoir are no-flow boundaries. These boundaries can be both sealing faults and nearby producing wells or fractures. During this period, the change in pressure at any place in the reservoir decreases at the same, constant rate. The reservoir is said to behave as a "tank".

ii. Steady state flow ($\partial p/dt = constant = 0$). Occurs when a constant pressure outer boundary exists (reservoir with aquifer or gas cap expansion support). During this period, the change in pressure at any place in the reservoir is zero.